10

Developments in Time-Frequency Analysis of Biomedical Signals and Images Using a Generalized Fourier Synthesis

Robert A. Brown, M. Louis Lauzon and Richard Frayne
McGill University and University of Calgary
Canada

1. Introduction

Quantitative time-frequency analysis was born with the advent of Fourier series analysis in 1806. Since then, the ability to examine the frequency content of a signal has become a critical capability in diverse applications ranging from electrical engineering to neuroscience. Due to the fundamental nature of the time-frequency transform, a great deal of work has been done in the field, and variations on the original Fourier transform (FT) have proliferated (Mihovilovic and Bracewell, 1991; Allen and Mills, 2004; Peyre and Mallat, 2005). While the FT (Allen and Mills, 2004) is an extremely important signal analysis tool, other related transforms, such as the short-time Fourier transform (STFT) (Allen and Mills, 2004), wavelet transform (WT) (Allen and Mills, 2004) and chirplet transform (Mihovilovic and Bracewell, 1991), have been formulated to address shortcomings in the FT when it is applied to certain problems. Considerable research has been undertaken in order to discover the properties of, and efficient algorithms for calculating the most important of these transforms.

The S-transform (ST) (Stockwell *et al.*, 1996; Mansinha *et al.*, 1997) is of interest as it has found several recent applications in medicine including image transmission (Zhu *et al.*, 2004), the study of psychiatric disorders (Jones *et al.*, 2006), early detection of multiple sclerosis lesions (Zhu *et al.*, 2001), identifying genetic abnormalities in brain tumours (Brown *et al.*, 2008), analysis of EEG recordings in epilepsy patients (Khosravani *et al.*, 2005) and analysis of ECG and audio recordings of cardiac abnormalities (Leung *et al.*, 1998). It has also been successfully applied to non-biomedical tasks such as characterizing the behaviour of liquid crystals (Özder *et al.*, 2007), detecting disturbances in electrical power distribution networks (Chilukuri and Dash, 2004), monitoring high altitude wind patterns (Portnyagin *et al.*, 2000) and detecting gravitational waves (Beauville *et al.*, 2005). However, the computational demands of the ST have limited its utility, particularly in clinical medicine (Brown *et al.*, 2005).

In this chapter we consider several of the more prominant transforms: the Fourier transform, short-time Fourier transform, wavelet transform, and S-transform. A general framework for describing linear time-frequency transforms is introduced, simplifying the direct comparison of these techniques. Using insights from this formalism, techniques developed for the Fourier and wavelet transforms are applied to the formulation of a fast discrete S-transform algorithm with greatly diminished computational and storage demands. This transform is much more computationally efficient than the original continuous approximation of the ST (Stockwell *et al.*, 1996) and so allows the ST to be used in acute clinical situations as well as allowing more advanced applications than have been investigated to date, including analyzing longer signals and larger images, as well as transforming data with three or more dimensions, *e.g.,* volumes obtained by magnetic resonance (MR) or computed tomography (CT) imaging. Finally, the STFT and ST are demonstrated in an example biomedical application.

The terminology is, unfortunately, inconsistent between the ST, wavelet and FT literatures. Though these inconsistencies will be pointed out when they arise, we will follow the wavelet convention, where the *continuous* transform takes as input a continuous signal and outputs a continuous spectrum, the *discrete approximation* transforms a discrete, sampled signal into a discrete, oversampled spectrum and the *discrete* transform converts a discrete signal into a discrete, critically sampled spectrum. Additionally, the term *fast* will be used to refer to computationally efficient algorithms for computing the discrete transform.

2. Overview of Selected Time-Frequency Transforms

2.1. The Fourier Transform

The Fourier transform converts any signal, $f(t)$, into its frequency spectrum, which represents the signal in terms of infinite complex sinusoids of different frequency, v, and phase:

$$F(v) = \int_{-\infty}^{+\infty} f(t) e^{-i2\pi vt} dt \tag{1}$$

The FT transforms entirely between the amplitude-time signal-space and the amplitude-frequency frequency-space. That is, the spectrum produced by the FT is necessarily global – it represents the average frequency content of the signal (Mansinha *et al.*, 1997). For stationary signals, where the frequency content does not change with time, this is ideal. However, most interesting biomedical signals are non-stationary: their frequency content does vary with time. However, the FT provides no information about this important property.

The FT, as with each of the transforms discussed in this section, is generalizable to any number of dimensions. Higher dimensional transforms may be used to analyze images (two-dimensional), volumetric data from tomographic medical scanners (three-dimensional) or volumetric scans over time (four-dimensional). Though the term "time-frequency" is commonly used, implying one-dimensional functions of amplitude versus time, these concepts are generalizable to higher dimensions and other parameters.

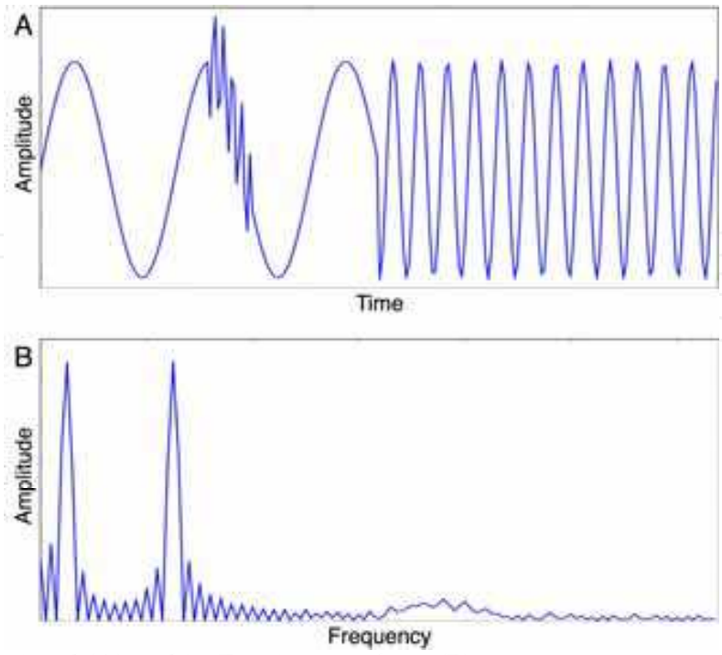

Fig. 1. A sample signal (A) and its Fourier transform (B).

The continuous FT can be calculated analytically according to Eq. (1) for many useful functions but computation of the FT for arbitrarily measured signals requires a discrete formulation. The discrete Fourier transform (Cooley *et al.*, 1969) (DFT) is calculated on a discretely sampled finite signal and provides a discretely sampled finite spectrum.

Simply evaluating the discrete form of Eq. (1) has a compuational complexity of $O(N^2)$. That is, the number of operations required to calculate the DFT grows approximately as the square of the signal length. The fast Fourier transform (Cooley and Tukey, 1965) (FFT) utilizes a divide-and-conquer approach to calculate the DFT more efficiently: it has a computational complexity of $O(N\log N)$. This difference means that computing the FFT of even short signals may be much faster than the DFT, so the FFT is almost universally preferred.

Fig. 1 shows a non-stationary test signal along with its discrete Fourier spectrum, calculated via the FFT algorithm. Note that Fourier spectra are normally complex-valued and include both positive and negative frequencies. For simplicity, figures in this chapter show the absolute value of the spectrum, and the positive-frequency half only. The test signal includes three frequency components: (1) a low frequency for the first half of the signal, (2) a higher frequency for the second half and (3) a very high burst added to the signal in the middle of the low frequency portion. The Fourier spectrum shows strong peaks corresponding to (1) and (2) but (3) is not well detected due to its short duration. Additionally, the sharp transitions between frequencies cause low-amplitude background throughout the spectrum. Note that the Fourier spectrum does not indicate the relative temporal positions of the frequency components.

2.2. The Short-Time Fourier Transform

The Gabor, or short-time Fourier transform (STFT) (Schafer and Rabiner, 1973), Eq. (2), improves Fourier analysis of non-stationary signals by introducing some temporal locality. The signal is divided into a number of partitions by multiplying with a set of window functions, $w(t-\tau)$, where τ indicates the centre of the window. In the case of the Gabor transform, this window is a Gaussian but the STFT allows general windows. In the simplest case, this window may be a boxcar, in effect, partitioning the signal into a set of shorter signals. Each partition is Fourier transformed, yielding the Fourier spectrum for that partition. The local spectra from each partition are combined to form the STFT spectrum, or spectrogram, which can be used to examine changes in frequency content over time.

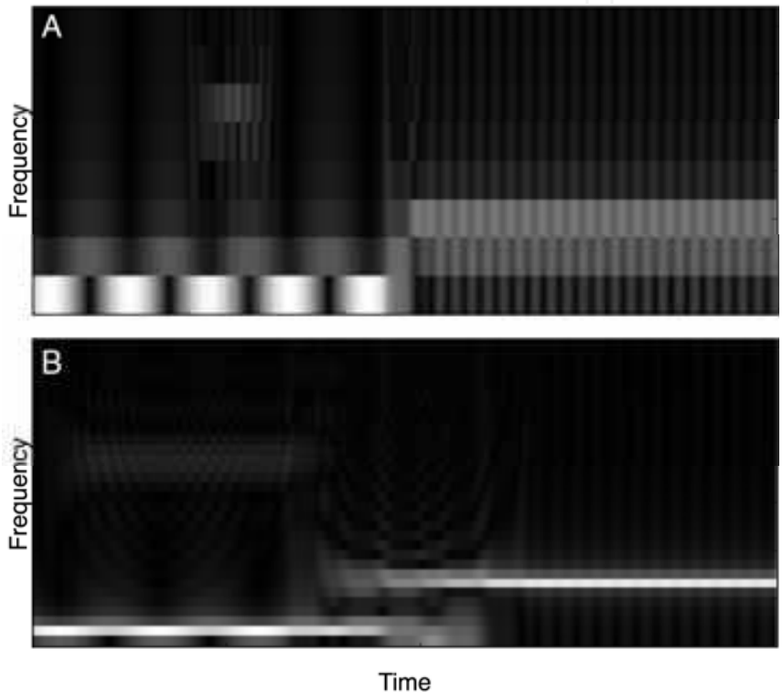

Fig. 2. The STFT of the signal in Fig. 1A with boxcar windows whose widths are 16 samples (A) and 32 samples (B).

$$F(\tau, v) = \int_{-\infty}^{+\infty} f(t) w(t-\tau) e^{-i2\pi vt} dt \tag{2}$$

Fig. 2 shows the STFT spectrum of the test signal in Fig. 1, using boxcar windows of two different widths. The STFT does provide information about which frequencies are present and where they are located, but this information comes at a cost. Narrower windows produce finer time resolution, but each partition is shorter. As with the FT, shorter signals produce spectra with lower frequency resolution. The tradeoff between temporal and frequency resolution is a consequence of the Heisenberg uncertainty principle (Allen and Mills, 2004):

$$\Delta t \Delta v \geq C \tag{3}$$

which states that the joint time and frequency resolution, $\Delta t \cdot \Delta \nu$, has a lower bound. Additionally, the Shannon sampling theorem (Shannon, 1949) requires that a wavelength be represented by more than two samples and, to avoid artifacts, the window must be wide enough to contain at least one wavelength. This means that lower frequencies are better represented by wider windows (sacrificing time resolution) while high frequencies benefit from narrower windows (sacrificing frequency resolution). In the STFT the window width is fixed so it must be chosen *a priori* to best reflect a particular frequency range of interest.

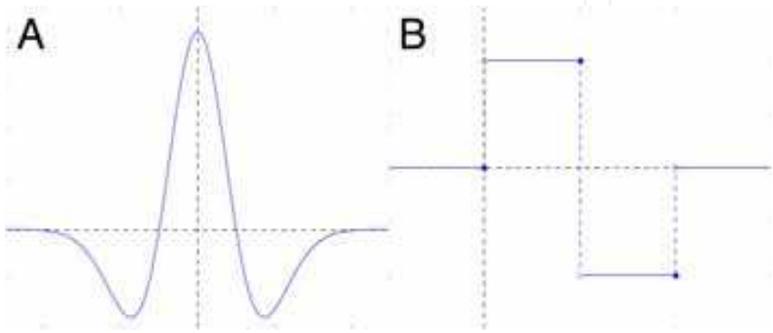

Fig. 3. Examples of two mother wavelets: (A) the continuous Ricker or Mexican hat wavelet and (B) the discrete Haar wavelet.

2.3. The Wavelet Transform

The obvious solution to the window-width dilemma associated with the STFT is to use frequency-adaptive windows, where the width changes depending on the frequency under examination. This feature is known as *progressive resolution* and has been found to provide a more useful time-frequency representation (Daubechies, 1990). Eq. (4) is the wavelet transform (Daubechies, 1990) (WT), which features progressive resolution:

$$\Psi(a,b) = \frac{1}{\sqrt{|a|}} \int_{-\infty}^{\infty} f(t) \psi\left(\frac{t-b}{a}\right) dt \tag{4}$$

where a is the dilation or scale factor (analogous to the reciprocal of frequency) and b is the shift, analogous to τ. The WT describes a signal in terms of shifted and scaled versions of a mother wavelet, $\psi\left(\frac{t-b}{a}\right)$, which is the analog of the complex sinusoidal basis functions used by the FT, but differs in that it is finite in length and is not a simple sinusoid. The finite length of the mother wavelet provides locality in the wavelet spectrum so windowing the signal, as with the STFT, is not necessary. Examples of two common mother wavelets are plotted in Fig. 3.

However, since the mother wavelet is not a sinusoid, the WT spectrum describes a measurement that is only related to frequency, usually referred to as scale, with higher

scales roughly corresponding to lower frequencies and *vice versa*. Additionally, since the mother wavelet is shifted during calculation of the WT, any phase measurements are local; i.e., they do not share a global reference point (Mansinha *et al.*, 1997).

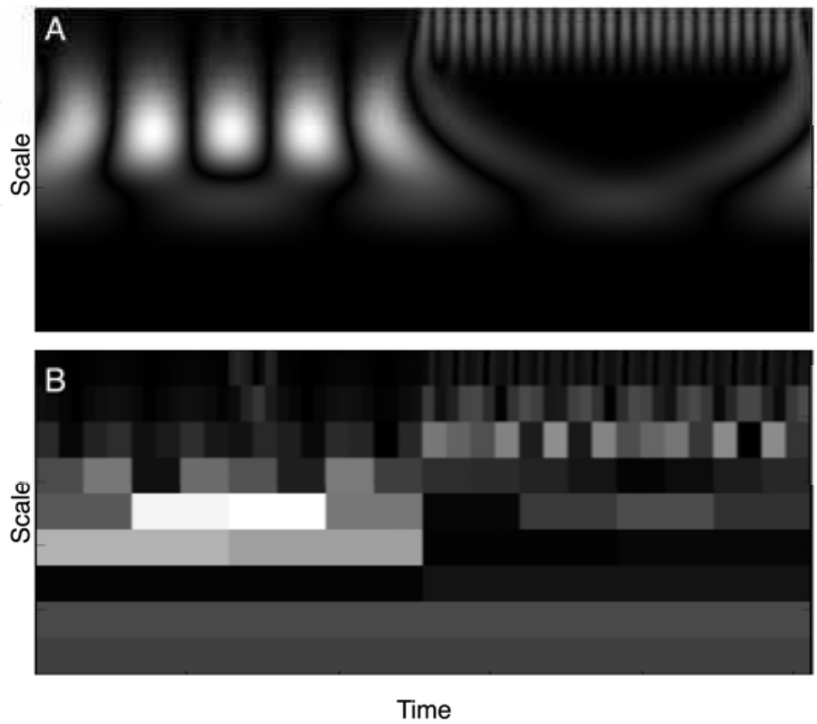

Fig. 4. The continuous Ricker (Mexican hat) wavelet transform (A) and discrete Haar wavelet transform (B) of the signal in Fig. 1A.

Some wavelets, such as the Ricker wavelet (Fig. 4A) or the Morlet wavelet, do not have well behaved discrete formulations and must be calculated using a discrete approximation of the continuous wavelet transform (CWT). This continous approximation is generally difficult to calculate and only practical for short signals of low dimension. However, many mother wavelets yield transforms that have discrete forms and can be calculated via the computationally efficient discrete wavelet transform (DWT). Some wavelets, such as the Haar (Allen and Mills, 2004), Fig. 4B, have a computational complexity of $O(N)$, even faster than the FFT (Beylkin *et al.*, 1991).

2.4. The S-Transform

The S-transform (Stockwell *et al.*, 1996; Mansinha *et al.*, 1997) (ST) combines features of the STFT and WT.

The ST is given by:

$$S(\tau,v)=\int_{-\infty}^{+\infty} f(t)\frac{|v|}{\sqrt{2\pi}}e^{-\frac{(t-\tau)^2 v^2}{2}}e^{-i2\pi vt}dt \tag{5}$$

which can be interpreted as an STFT that utilizes a frequency-adaptive, Gaussian window, providing progressive resolution. Alternatively, the ST can be derived as a phase correction to the Morlet wavelet, yielding a wavelet-like transform that provides frequency and globally referenced phase information. The ST of the test signal in Fig. 1 is shown in Fig. 5.

Unfortunately, these advantages come at a cost. The Morlet wavelet must be calculated via the inefficient CWT. Similarly, the continuous approximation of the ST in Eq. (5) has a computational complexity of $O(N^3)$. A more efficient algorithm, however, is described in Eq. (6), in which the ST is calculated from the Fourier transform of the signal (Stockwell *et al.*, 1996):

$$S(\tau,v)=\int_{-\infty}^{+\infty} F(\mu+v)e^{-\frac{2\pi^2\mu^2}{v^2}}e^{i2\pi\tau\mu}d\mu \tag{6}$$

where $F(\mu+\nu)$ is the Fourier transform of the signal, and it is multiplied by a Gaussian and the inverse Fourier transform kernel. The integration is over frequency, μ. In this form, the ST can be calculated using the FFT but this algorithm is still $O(N^2\log N)$. Additionally, the ST requires $O(N^2)$ units of storage for the transform result, while the DFT and DWT require only $O(N)$. For a 256×256 pixel, 8-bit complex-valued image, which requires 128 kilobytes of storage, the DFT or DWT will occupy no more space than the original signal. But, the ST will require 8 gigabytes of storage space. Either the compuational complexity, memory requirements or both quickly make calculation of the ST for larger signals prohibitive. Addressing these problems is a prerequisite for most clinical applications and also for practical research using the ST.

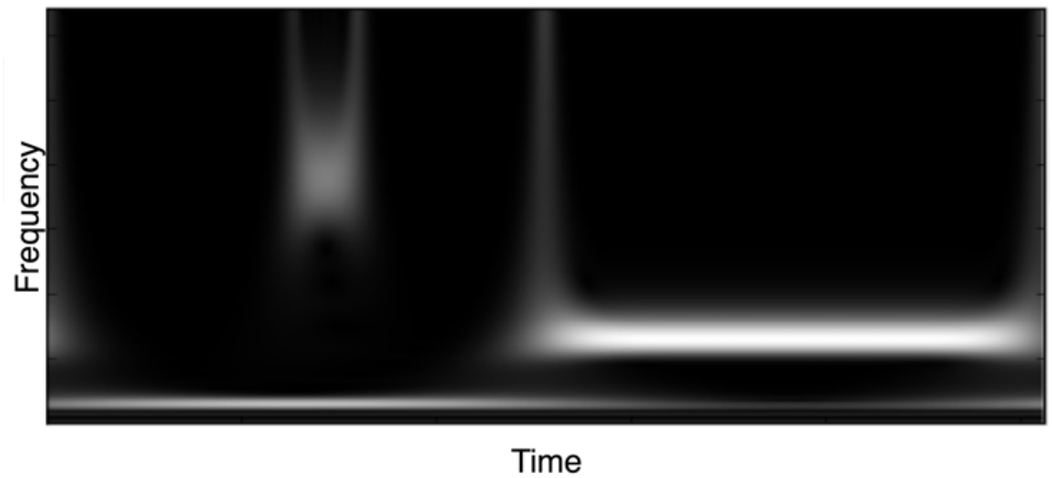

Fig. 5. The ST of the signal in Fig. 1A.

Further discussion of the transforms covered in this section, along with illustrative biomedical examples, can be found in (Zhu *et al.*, 2003).

3. General Transform

Though the different transforms, particularly the Fourier and wavelet transforms, are often considered to be distinct entities, they have many similarities. To aid comparison of the ST with other transforms and help translate techniques developed for one transform to be used with another, we present several common transforms in a unified context. Previous investigators have noted the similarities between the FT, STFT and wavelet transform and the utility of representing them in a common context. To this end, generalized transforms that describe all three have been constructed (Mallat, 1998; Qin and Zhong, 2004). However, to our knowledge, previous generalized formalisms do not explicitly specify separate kernel and window functions. Separating the two better illustrates the relationships between the transforms, particularly when the ST is included.

The ST itself has been generalized (Pinnegar and Mansinha, 2003):

$$S(\tau,v)=\int_{-\infty}^{+\infty} f(t)w(t-\tau,v)e^{-i2\pi vt}dt \tag{7}$$

This generalized S-transform (GST) admits windows of arbitrary shape. It may additionally be argued that $w(t-\tau,\nu)$ can be defined such that the window does not depend on the parameter ν. The result is a fixed window width for all frequencies, and the transform becomes a STFT. However, the presence of ν in the parameter list is limiting and we prefer the following more general notation:

$$S(\tau,v)=\int_{-\infty}^{+\infty} f(t)w(t-\tau,\sigma)e^{-i2\pi vt}dt \tag{8}$$

where σ may be chosen to be equal to ν, to perform an ST, or may be a constant, producing an STFT. In the latter case, if $w(t-\tau,\sigma)=1$, the transform is an FT. Thus, Eq. (8) is a general Fourier-family transform (GFT), describing each of the transforms that utilize the Fourier kernel.

3.1. Extension to the Wavelet Transform

The wavelet transform, though it accomplishes a broadly similar task, at first glance appears to be very disctinct from the Fourier-like time-frequency transforms. The WT uses basis functions that are finite and can assume various shapes, many of which look very unusual compared to the sinusoids described by the Fourier kernel. However, when the basis function is decomposed into its separate kernel and window functions, the WT can be united with the Fourier-based transforms.

Consider the wavelet transform, defined in Eq. (4). Let $g(t)=\frac{\psi(t)}{e^{-i2\pi t}}$, that is, a version of the mother wavelet divided by a phase ramp. For a shifted and scaled wavelet, this becomes:

$$g\left(\frac{t-b}{a}\right)=\frac{\psi\left(\frac{t-b}{a}\right)}{e^{-\frac{i2\pi(t-b)}{a}}} \tag{9}$$

Rearranging and substituting into Eq. (4) yields:

$$\Psi(a,b)=\frac{1}{\sqrt{|a|}}\int_{-\infty}^{\infty}f(t)g\left(\frac{t-b}{a}\right)e^{-\frac{i2\pi(t-b)}{a}}dt \tag{10}$$

The complex exponential term can be expanded into two terms, one of which is similar to the familiar Fourier kernel:

$$\Psi(a,b)=\frac{1}{\sqrt{|a|}}\int_{-\infty}^{\infty}f(t)g\left(\frac{t-b}{a}\right)e^{\frac{i2\pi b}{a}}e^{-\frac{i2\pi t}{a}}dt \tag{11}$$

Letting $\tau = b$, $\nu=\frac{1}{a}$, and $S(\nu,\tau)=\Psi\left(\frac{1}{\nu},\tau\right)$, this becomes:

$$\Psi(a,b)=S(v,\tau)=\sqrt{|v|}\int_{-\infty}^{\infty}f(t)g\left(v\left[t-\tau\right]\right)e^{i2\pi v\tau}e^{-i2\pi vt}dt \tag{12}$$

Finally, letting $w(t-\tau,\nu)=g(\nu[t-\tau])\sqrt{|\nu|}e^{i2\pi\nu\tau}$, Eq. (12) becomes the GFT, Eq. (8), with σ=ν. Substituting the Fourier-style variables into Eq. (9), rearranging and simplifying gives the window function in terms of the mother wavelet:

$$w(t,\tau,v)=\sqrt{|v|}\psi\left(v\left[t-\tau\right]\right)e^{i2\pi vt} \tag{13}$$

Thus, the wavelet transform can also be described as a GFT.

4. The Fast S-Transform

Though calculating a discrete approximation of a continuous transform is useful, as with the continuous wavelet and S-transforms, a fully discrete approach makes optimal use of knowledge of the sampling process applied to the signal to decrease the computational and memory resources required. In this section a discrete fast S-transform (FST) (Brown and Frayne, 2008) is developed by utilizing properties that apply to all of the discrete versions of transforms described by the GFT, Eq. (8).

A sampled signal has two important features – the sampling period, Δt, and the number of samples, N. Multiplying these two values gives the total signal length, W_t. Sampling the signal and limiting it to finite length imposes several limitations on the transformed spectrum. The Fourier transform is the simplest case. The DFT of a signal is limited to the same number of samples, N, as the original signal, conserving the information content of the signal. The highest frequency that can be represented, $\nu_{\max}$, is the Nyquist frequency, which is half the signal sampling frequency, $\frac{1}{2\Delta t}$. The sampling period of the frequency spectrum, $\Delta\nu$, is the reciprocal of the signal length, $1/W_t$.

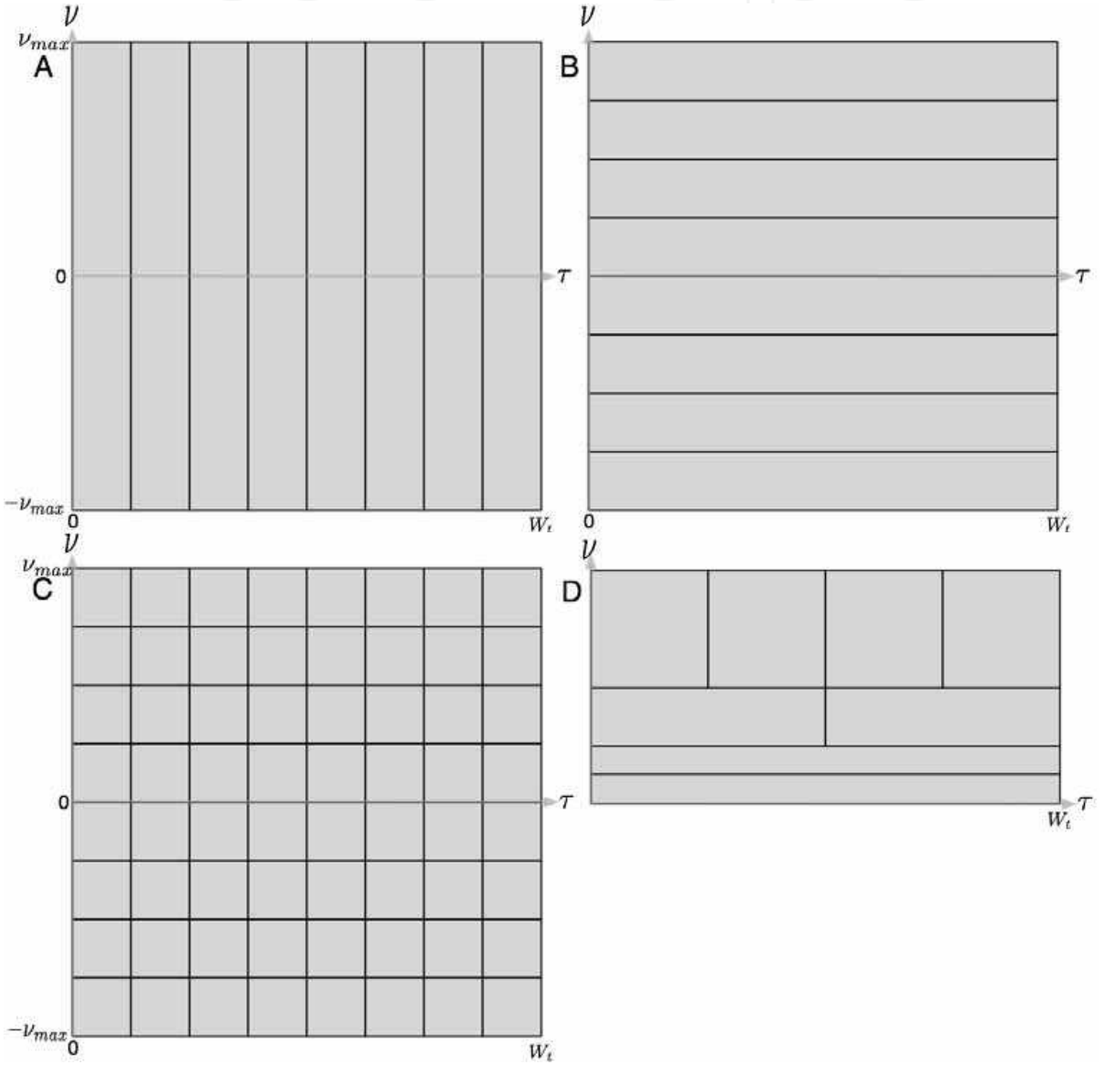

Fig. 6. ν-τ sampling scheme for (A): a uniformly sampled signal with N = 8, (B): the Fourier transform, (C): the conventional S-transform and (D): a discrete Wavelet transform.

Ideally, the result of the continuous S-transform of a one-dimensional signal is $S(\tau,\nu)$, a spectrum with both time and frequency axes. A fast ST must sample the τ-ν plane sufficiently such that the transform can be inverted (*i.e.*, without loss of information) but also avoid unnecessary oversampling. If the original signal contains N points, we possess N independent pieces of information. Since information cannot be created by a transform (and must be conserved by an invertible transform) an efficient ST will produce an N-point spectrum, as does the DFT. The original definition of the ST produces a spectrum with N^2 points. Therefore, for all discrete signals where $N>1$, the continuous ST is oversampled by a factor of N.

In addition, the ST varies temporal and frequency resolution for different frequencies under investigation: higher frequency/lower time resolution at low frequencies and the converse at higher frequencies, but this is not reflected in the uniform N^2-point τ-ν plane sampling scheme. According to the uncertainty principle, at higher frequencies the FST should produce τ-ν samples that have a lesser resolution along the frequency axis and greater resolution along the time axis, in analogy to the DWT. The cost of this oversampling is evident in the increased computational complexity and memory requirements of the ST.

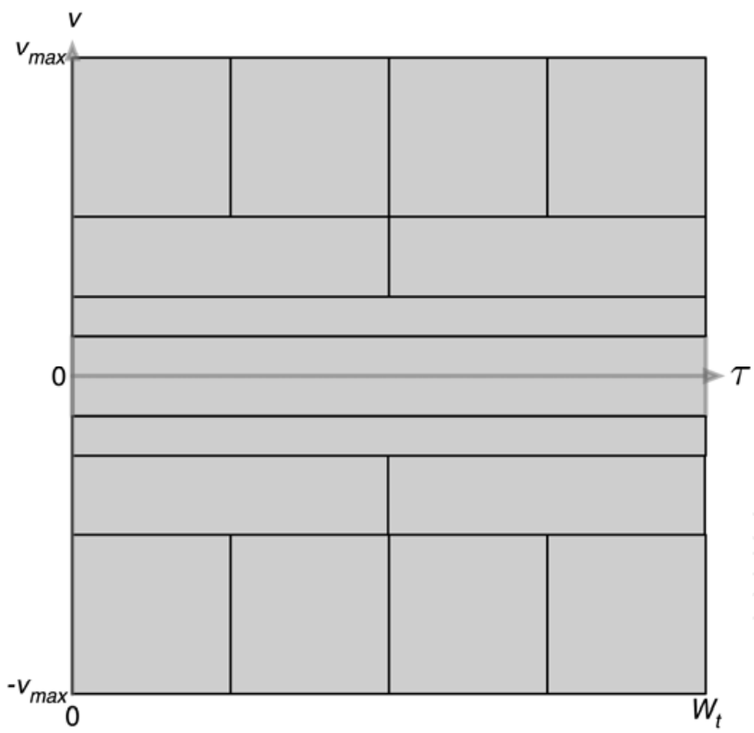

Fig. 7. Sampling scheme for the discrete S-transform of a complex 8-sample signal.

The dyadic sampling scheme used by discrete wavelet transforms provides a progressive sampling scheme that matches underlying resolution changes. In light of the similarities between the DWT and ST illustrated by the GFT, a dyadic sampling scheme can be used to construct a discrete ST. In the case of the ST of a complex signal, a double dyadic scheme is

necessary to cover both the positive and negative frequency ranges. In this arrangement, time resolution is at a minimum for low frequencies, both positive and negative, and increases with the absolute value of frequency. For comparision, the τ-ν plane sampling schemes for the signal, FT, continuous (*i.e.*, conventional) ST and DWT are shown in Fig. 6. The double dyadic scheme of the FST is illustrated in Fig. 7, and a particular algorithm for calculating the FST with this type of sampling scheme is presented in Algorithm 1. The result from Algorithm 1 is presented for a sample signal in Fig. 8.

As might be expected from the GFT formalism, Algorithm 1 is very similar to a filterbank DWT algorithm. High- and low-pass filters, applied in the frequency domain, divide the signal into high- and-low frequency halves (often called "detail" and "approximation", respectively, in the wavelet literature). The high frequency portion is then multiplied by the necessary windowed kernel functions. The low frequency portion forms the input to the next iteration of the algorithm, where it is further decomposed. This simple arrangement produces a dyadic scale with a strict power of two pattern, but can be modified by adjusting the filters to produce finer or coarser frequency domain sampling. However, care must be taken to appropriately modify the time domain sampling to match, and never to violate the Nyquist criterion.

The Gaussian windows of the ST are effectively infinite in extent but when calculating the transform of a finite length signal, the Gaussians are necessarily multiplied by a boxcar window the width of the signal itself. Therefore, the actual window for any finite length signal is a Gaussian multiplied by a boxcar. This situation is particularly apparent at lower frequencies, where the Gaussians are wider and may still be of appreciable amplitude when they are clipped at the edges of the signal. In the discrete approximation of the continuous ST, the Gaussian window is scaled with frequency but the boxcar is not. This contrasts with the Morlet wavelet, which, using the general formalism of Eq. (8), can also be defined with a window that is a composite of a Gaussian and a boxcar. However, in the Morlet wavelet, the Gaussian and boxcar are scaled together. This joint scaling is also inherent in the FST algorithm. Scaling of both parts of the window function is a key refinement, as it both produces more consistent windows and significantly decreases the computational complexity of the FST.

It is only necessary to compute the sums in step 5 of Algorithm 1 for non-zero points (those that are inside the boxcar window). The boxcar must always be wide enough to contain at least one entire wavelength, but the width does not need to be a multiple of the wavelength. This effectively decreases W_t: the full signal length is required only for calculating the DC component, and shorter portions are used at higher frequencies. Since we are downsampling in step 4, Δt is smallest at high frequencies and becomes progressively larger at lower frequencies and so the summation operation in step 5 will always be over a constant number of points. The examples in this paper use 4 points, which produces a slightly oversampled, but smoother, result. This reduces the complexity of step 5, which is nested inside two FOR loops, from $O(N)$ to constant complexity: $O(C)$. As an additional benefit, adjusting the width of the boxcar window greatly reduces the number of kernels and windows that must be pre-calculated in steps 2 and 3 of Algorithm 1, since the kernels

and windows remain essentially constant while the signal's length and resolution are manipulated.

Algorithm 1: The Discrete S-Transform with 2x Oversampling

1. Calculate the Fourier transform of the signal, $H\left(\frac{n}{NT}\right)$

2. Pre-calculate the required kernel functions:

$\phi^{+} = (kT, \frac{n}{NT}) = e^{-\frac{i2\pi kn}{N}}$ and $\phi^{-} = (kT, \frac{n}{NT}) = e^{\frac{i2\pi kn}{N}}$

3. Pre-calculate the window functions: $w(kT, \frac{n}{NT})$

FOR n in $\{\frac{N}{2}, \frac{N}{4}, \frac{N}{8}, ..., 4, 2, 1\}$ DO:

4. Band pass filter $H(\kappa)$:

$$H'(\kappa) = H(\kappa) \text{ where } \frac{n}{2} < |\kappa| \le n$$

and inverse FT to obtain $h'(t)$.

FOR every point j in $h'(t)$ DO:

5. Calculate the transform samples:

$$S(jT, \frac{3n}{4NT}) = \sum_{k=0}^{N-1} h'(kT) \cdot w(kT - T, \left|\frac{3n}{4NT}\right|) \cdot \phi^{+}(kT, \frac{3n}{4NT})$$

$$S(jT, -\frac{3n}{4NT}) = \sum_{k=0}^{N-1} h'(kT) \cdot w(kT - T, \left|\frac{3n}{4NT}\right|) \cdot \phi^{-}(kT, \frac{3n}{4NT})$$

END FOR

END FOR

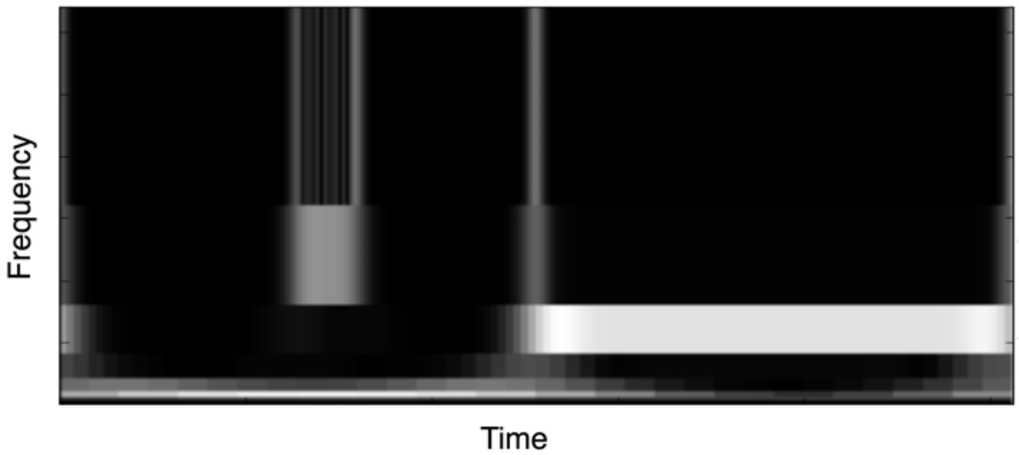

Fig. 8. The fast discrete ST of the signal in Fig. 1A.

The computational complexity of the FST algorithm is $O(NlogN)$ – the same as that of the Fourier transform. The storage requirements are $O(N)$, like the FFT and discrete wavelet transforms (Brown and Frayne, 2008).

5. The Inverse Fast S-Transform

A discrete version of the S-transform should be invertible by the same procedure as the inverse continuous ST: summation of the transform space over the τ-axis, producing the Fourier spectrum, which can then be inverse discrete or fast Fourier transformed to obtain the original signal. The inverse discrete and fast Fourier transforms require a coefficient for each integer value of the frequency index variable ν from $-\frac{\nu_{\max}}{2}$ to $+\frac{\nu_{\max}}{2}$. Since the FST uses an octave (*i.e.*, dyadic) system along the ν-axis, the missing coefficients must be calculated from known points and *a priori* information. Note that the following derivation uses the general definition for the window, $w(t-\tau,\sigma)$. In the specific case of the FST, $\sigma = \nu_p$.

Consider a single line of the GFT spectrum for ν fixed at some value ν_p: $l(\tau) = S(\tau, \nu_p)$. Then, from Eq. (8):

$$l(\tau) = S(\tau, v_p) = \int_{-\infty}^{+\infty} f(t) w(t-\tau,\sigma) e^{-i2\pi v_p t} dt \tag{14}$$

The Fourier transform of $l(\tau)$, $L(\nu')$ is:

$$L(v') = \int_{-\infty}^{\infty} \left\{ \int_{-\infty}^{+\infty} f(t) w(t-\tau,\sigma) e^{-i2\pi v_p t} dt \right\} e^{-i2\pi\tau v'} d\tau \tag{15}$$

Rearranging terms gives:

$$L(v') = \int_{-\infty}^{+\infty} f(t) e^{-i2\pi v_p t} dt \int_{-\infty}^{\infty} w(t-\tau,\sigma) e^{-i2\pi\tau v'} d\tau \tag{16}$$

Evaluating the second integral using the Fourier shift theorem, this becomes:

$$L(v') = \int_{-\infty}^{+\infty} f(t) e^{-i2\pi v_p t} dt \left[W^*(v',\sigma) e^{-i2\pi t v'} \right] \tag{17}$$

where $W^*(\nu',\sigma)$ is the inverse Fourier transform of the window. In the common case where the window function is real and even the inverse and forward FT are identical, in which case $W^*(\nu',\sigma)$ is interchangeable with $W(\nu',\sigma)$, the forward Fourier transform of the window. This can be rearranged to give:

$$L(v') = W^*(v',\sigma) \int_{-\infty}^{+\infty} f(t) e^{-i2\pi v_p t} e^{-i2\pi t v'} dt \tag{18}$$

Evaluating the integral, which is a Fourier transform, gives:

$$L(v') = W^*(v',\sigma) F(v' + v_p) \tag{19}$$

Finally, after rearranging:

$$F(v' + v_p) = \frac{L(v')}{W^*(v',\sigma)} \tag{20}$$

It is clear that, in the continuous case, any Fourier coefficient can be obtained from the Fourier transform of any fixed $\nu = \nu_p$ line of the GFT spectrum. In the discrete, fast transform case, as calculated by Algorithm 1, recall that the Fourier spectrum is band pass filtered during computation of $S(\tau, \nu_p)$. This means that the Fourier spectrum retrieved from Eq. (20) will also be filtered. However, as each $\nu = \nu_p$ line results from a *different* band pass filtering, the full Fourier spectrum can be reconstructed from the $S(\tau, \nu_p)$ spectrum via Eq. (20). It is then a simple matter to perform an inverse FFT and reconstruct the original signal. Note that the inversion procedure for the continuous approximation of the ST (Mansinha *et al.*, 1997), summation over the τ-axis, is equivalent to applying Eq. (20) to each line but discarding all but the DC component, $F(\nu' + \nu_p)$ where $\nu' = 0$.

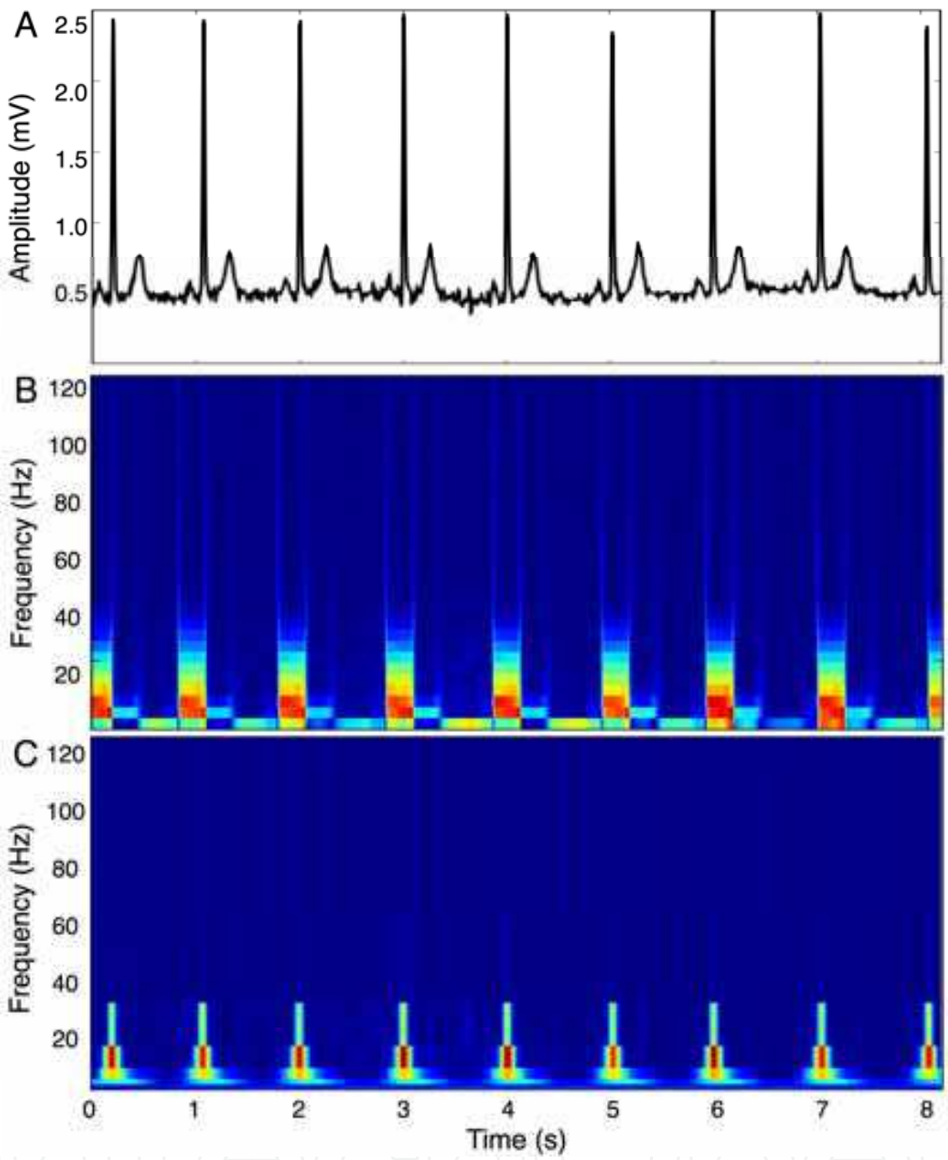

Fig. 9. A short segment of an electrocardiogram (A), its STFT (B) and FST (C). Red indicates high power while blue indicates low power.

6. Biomedical Example

Fig. 9 shows a sample biomedical signal, along with its STFT and FST. The signal (Fig. 9A) is a short electrocardiogram (ECG) recording from a publicly available subset of the European ST-T Database (Physionet, http://pysionet.org), consisting of the first 2048 samples from the V4 lead of record e0103, a 62 year old male subject complaining of mixed angina. Although the STFT (Fig. 9B) and the FST (Fig. 9C) both provide spectra on the time-frequency plane, their respective temporal-frequency resolutions are very different. The window width of the STFT is fixed for all frequencies, in this case at 64 points, yielding the same combination of

time and frequency resolution in all parts within the spectrum. In contrast, the FST demonstrates progressive resolution, trading decreased frequency resolution for increased time resolution at higher frequencies.

This difference is most obvious in the major spectral features corresponding to the R-waves (the dominant peaks in the ECG signal, which are associated with depolarization of the ventricles). In the STFT spectrum, localisation of the R-wave peak is limited by the time resolution of the transform. In this case, the peak can only be approximately located. Note also that the low frequency features corresponding to the other characteristic ECG components that occur between R-waves appear in the lowest frequency band of the STFT. Using this window, these features are not distinguishable from the DC, or zero-frequency component. In order to show these features, the DC component was removed from the signal before transforming.

In the FST spectrum, the R-wave can be localized much more precisely by examining higher frequencies, between 20 and 40 Hz, where the time resolution is much better. At the same time, increased frequency resolution at lower frequencies in the FST spectrum has allowed low frequency features to be better resolved and separated from the DC component.

The example signal in Fig. 9 consists of few samples and it can be transformed in a reasonable time even with the inefficient continuous approximation of the ST: the ST takes 1.6 s and 64 MB compared to 1.7 ms and 2 KB for the FST (2.5 GHz Intel Core 2 Duo, one core only). However, the full ECG signal consists of almost two million samples. Higher dimensional datasets, including medical images and volumes, can be even larger. ST and FST computation times and memory requirements for a few biomedical signals are compared in Table 1.

		ST		FST	
	Samples	Time	Memory	Time	Memory
MR Image	256 × 256	40 min	64 GB	40 ms	1 MB
CT Image	1024 × 1024	9 days	16 TB	0.8 s	16 MB
ECG	2^{21}	37 days	64 TB	1.7 s	32 MB
MR Volume	256 × 256 × 64	156 days	256 TB	3.6 s	64 MB
Visible Human (male) CT	512 × 512 × 1871	7.6 thousand years	3 EB	9 minutes	7 GB

Table 1. Approximate computation times and memory requirements for (i) the continuous approximation of the ST and (ii) the FST of various biomedical signals. These estimates are based on computations using one core of a 2.5 GHz Intel Core 2 Duo processor.

7. Conclusions

In this chapter we have defined a generalized framework that describes time-frequency transforms, including the familiar Fourier and wavelet transforms, in unified terms. Using

the generalized framework as a guide, we examined the ST, a transform that has proven to be particularly useful in biomedical and medical applications as well as in non-medical fields. A discrete fast implementation of the ST, the FST, was derived, which has a computational complexity of $O(NlogN)$ and memory complexity of $O(N)$, a significant improvement on the continuous approximation of the ST computational complexity of $O(N^2logN)$ and storage complexity of $O(N^2)$. This decrease in complexity allows calculation of the FST, with modest resources, of signals of more than 2^{16} points, *i.e.*, images larger than 256x256 pixels, volumes, and higher dimensional datasets of non-trivial size. The increased efficiency and wider applicability of the FST allows it to be considered for more applications, including those that have strict size or time limitations such as compression, progressive image transmission or acute care medical image analysis.

8. References

Allen, R. L. & Mills, D. W. (2004). *Signal Analysis,* IEEE Press, 0-471-23441-9, Piscataway, NJ

Beauville, F.; Bizouard, M. A.; Bosi, L.; Brady, P.; Brocco, L.; Brown, D.; Buskulic, D.; Chatterji, S.; Christensen, N.; Clapson, A. C.; Fairhurst, S.; Grosjean, D.; Guidi, G.; Hello, P.; Katsavounidis, E.; Knight, M.; Lazzarini, A.; Marion, F.; Mours, B.; Ricci, F.; Viceré, A. & Zanolin, M. (2005). A first comparison of search methods for gravitational wave bursts using LIGO and VIRGO simulated data. *Classical and Quantum Gravity*, 22, (2005) S1293-S1301

Beylkin, G.; Coifman, R. & Rokhlin, V. (1991). Fast wavelet transforms and numerical algorithms I. *Communications on Pure and Applied Mathematics*, 44, 2, (1991) 141-183

Brown, R.; Zhu, H. & Mitchell, J. R. (2005). Distributed vector processing of a new local multi-scale Fourier transform for medical imaging applications. *IEEE Transactions on Medical Imaging*, 24, 5, (2005) 689-691

Brown, R. A. & Frayne, R. A fast discrete S-transform for biomedical signal processing, *IEEE Engineering in Medicine and Biology Conference*, Vancouver, BC, 2008

Brown, R. A.; Zlatescu, M. C.; Sijben, A.; Roldan, G.; Easaw, J.; Forsyth, P. A.; Parney, I.; Sevick, R. A.; Yan, E.; Demetrick, D.; Schiff, D.; Cairncross, J. G. & Mitchell, J. R. (2008). The use of magnetic resonance imaging to noninvasively detect genetic signatures in oligodendroglioma. *Clinical Cancer Research*, 14, (2008) 2357-2362

Chilukuri, M. V. & Dash, P. K. (2004). Multiresolution S-transform-based fuzzy recognition system for power quality events. *IEEE Transactions on Power Delivery*, 19, (2004) 323-330

Cooley, J. W. & Tukey, J. W. (1965). An algorithm for the machine calculation of complex Fourier series. *Mathematics of Computation*, 19, (1965) 297-301

Cooley, J. W.; Lewis, P. A. W. & Welch, P. D. (1969). The finite Fourier transform. *IEEE Transactions on Audio and Electroacoustics*, 17, 2, (1969) 77-85

Daubechies, I. (1990). The wavelet transform, time-frequency localization and signal analysis. *IEEE Transactions on Information Theory*, 36, 5, (1990) 961-1005

Jones, K. A.; Porjesz, B.; Chorlian, D.; Rangaswamy, M.; Kamarajan, C.; Padmanabhapillai, A.; Stimus, A. & Begleiter, H. (2006). S-transform time-frequency analysis of p300 reveals deficits in individuals diagnosed with alcoholism. *Clinical Neurophysiology*, 117, 10, (2006) 2128-2143

Khosravani, H.; Pinnegar, C. R.; Mitchell, J. R.; Bardakjian, B. L.; Federico, P. & Carlen, P. (2005). Increased high-frequency oscillations precede in vitro low Mg2+ seizures. *Epilepsia*, 46, 8, (2005) 1188-1197

Leung, T. S.; White, P. R.; Cook, J.; Collis, W. B.; Brown, E. & Salmon, A. P. (1998). Analysis of the second heart sound for diagnosis of paediatric heart disease. *IEE Proceedings on Science, Measurement and Technology*, 145, 6, (1998) 285-290

Mallat, S. G. (1998). *A Wavelet Tour of Signal Processing,* Academic Press,

Mansinha, L.; Stockwell, R. & Lowe, R. (1997). Pattern analysis with two-dimensional spectral localisation: Applications of two-dimensional S-transforms. *Physica A*, 239, (1997) 286-295

Mihovilovic, D. & Bracewell, R. N. (1991). Adaptive chirplet representation of signals in the time-frequency plane. *Electronics Letters*, 27, 13, (1991) 1159-1161

Özder, S.; Coşkun, E.; Köysal, O. & Kocahan, Ö. (2007). Determination of birefringence dispersion in nematic liquid crystals by using an S-transform. *Optics Letters*, 32, (2007) 2001-2003

Peyre, G. & Mallat, S. (2005). Surface compression with geometric bandelets. *ACM Transactions on Graphics*, 24, 3, (2005) 601-608

Pinnegar, C. R. & Mansinha, L. (2003). The S-transform with windows of arbitrary and varying shape. *Geophysics*, 68, (2003) 381-385

Portnyagin, Y. I.; Forbes, J.; Merzlyakov, E. G.; Makarov, N. A. & Palo, S. E. (2000). Intradiurnal wind variations observed in the lower thermosphere over the south pole. *Annales Geophysicae*, 18, (2000) 547-554

Qin, S. R. & Zhong, Y. M. (2004). Research on the unified mathematical model for FT, STFT and WT and its applications. *Mechanical Systems and Signal Processing*, 18, 6, (2004) 1335-1347

Schafer, R. W. & Rabiner, L. R. (1973). Design and simulation of a speech analysis-synthesis system based on short-time Fourier analysis. *IEEE Transactions on Audio and Electroacoustics*, AU-21, 3, (1973) 165-174

Shannon, C. E. (1949). Communication in the presence of noise. *Proceedings of the I.R.E.*, 37, 1, (1949) 10-21

Stockwell, R. G.; Mansinha, L. & Lowe, R. P. (1996). Localization of the complex spectrum: The S transform. *IEEE Transactions on Signal Processing*, 44, 4, (1996) 998-1001

Zhu, H.; Mayer, G.; Mansinha, L.; Law, A. G.; Archibald, C. J.; Metz, L. & Mitchell, J. R. Space-local spectral texture map based on MR images of MS patients, *MS: Clinical and Laboratory Research, ACTRIMS*, Chicago, 2001

Zhu, H.; Goodyear, B. G.; Lauzon, M. L.; Brown, R. A.; Mayer, G. S.; Law, A. G.; Mansinha, L. & Mitchell, J. R. (2003). A new local multiscale Fourier analysis for medical imaging. *Medical Physics*, 30, 6, (2003) 1134-1141

Zhu, H.; Brown, R. A.; Villanueva, R. J.; Villanueava-Oller, J.; Lauzon, M. L.; Mitchell, J. R. & Law, A. G. (2004). Progressive imaging: S-transform order. *Australian and New Zealand Industrial and Applied Mathematics Journal*, 45, (2004) C1002-1016

IntechOpen

Recent Advances in Biomedical Engineering

Edited by Ganesh R Naik

ISBN 978-953-307-004-9
Hard cover, 660 pages
Publisher InTech
Published online 01, October, 2009
Published in print edition October, 2009

The field of biomedical engineering has expanded markedly in the past ten years. This growth is supported by advances in biological science, which have created new opportunities for development of tools for diagnosis and therapy for human disease. The discipline focuses both on development of new biomaterials, analytical methodologies and on the application of concepts drawn from engineering, computing, mathematics, chemical and physical sciences to advance biomedical knowledge while improving the effectiveness and delivery of clinical medicine. Biomedical engineering now encompasses a range of fields of specialization including bioinstrumentation, bioimaging, biomechanics, biomaterials, and biomolecular engineering. Biomedical engineering covers recent advances in the growing field of biomedical technology, instrumentation, and administration. Contributions focus on theoretical and practical problems associated with the development of medical technology; the introduction of new engineering methods into public health; hospitals and patient care; the improvement of diagnosis and therapy; and biomedical information storage and retrieval. The book is directed at engineering students in their final year of undergraduate studies or in their graduate studies. Most undergraduate students majoring in biomedical engineering are faced with a decision, early in their program of study, regarding the field in which they would like to specialize. Each chosen specialty has a specific set of course requirements and is supplemented by wise selection of elective and supporting coursework. Also, many young students of biomedical engineering use independent research projects as a source of inspiration and preparation but have difficulty identifying research areas that are right for them. Therefore, a second goal of this book is to link knowledge of basic science and engineering to fields of specialization and current research. The editor would like to thank the authors, who have committed so much effort to the publication of this work.

Slavka Krautzeka 83/A
51000 Rijeka, Croatia
Phone: +385 (51) 770 447
Fax: +385 (51) 686 166
www.intechopen.com

No.65, Yan An Road (West), Shanghai, 200040, China
中国上海市延安西路65号上海国际贵都大饭店办公楼405单元
Phone: +86-21-62489820
Fax: +86-21-62489821

IntechOpen

IntechOpen